

Brillouin resonance broadening due to structural variations in nanoscale waveguides

C. Wolff,^{1,2} R. Van Laer,^{3,4} M. J. Steel,^{1,5} B. J. Eggleton,^{1,6} and C. G. Poulton^{1,2}

¹*Centre for Ultrahigh bandwidth Devices for Optical Systems (CUDOS),*

²*School of Mathematical and Physical Sciences, University of Technology Sydney, NSW 2007, Australia*

³*Photonics Research Group, Ghent University–imec, Belgium*

⁴*Center for Nano- and Biophotonics, Ghent University, Belgium*

⁵*MQ Photonics Research Centre, Department of Physics and Astronomy,
Macquarie University Sydney, NSW 2109, Australia*

⁶*Institute of Photonics and Optical Science (IPOS),
School of Physics, University of Sydney, NSW 2006, Australia*

(Dated: December 21, 2021)

We study the impact of structural variations (that is slowly varying geometry aberrations and internal strain fields) on the width and shape of the stimulated Brillouin scattering (SBS) resonance in nanoscale waveguides. We find that they lead to an inhomogeneous resonance broadening through two distinct mechanisms: firstly, the acoustic frequency is directly influenced via mechanical nonlinearities; secondly, the optical wave numbers are influenced via the opto-mechanical nonlinearity leading to an additional acoustic frequency shift via the phase-matching condition. We find that this second mechanism is proportional to the opto-mechanical coupling and, hence, related to the SBS-gain itself. It is absent in intra-mode forward SBS, while it plays a significant role in backward scattering. In backward SBS increasing the opto-acoustic overlap beyond a threshold defined by the fabrication tolerances will therefore no longer yield the expected quadratic increase in overall Stokes amplification. Finally, we illustrate in a numerical example that in backward SBS and inter-mode forward SBS the existence of two broadening mechanisms with opposite sign also opens the possibility to compensate the effect of geometry-induced broadening. Our results can be transferred to other micro- and nano-structured waveguide geometries such as photonic crystal fibres.

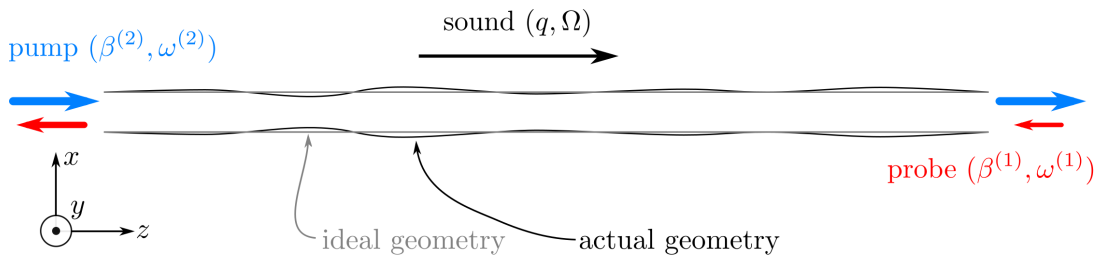


FIG. 1. Sketch of the basic setup studied in this manuscript using the case of backward SBS and geometric variations of a simple rectangular waveguide as an example: An optical pump (superscript 2) and an optical probe (superscript 1) excite a sound wave inside a waveguide that is assumed to be smooth, but whose geometry is smoothly and slowly perturbed along the axis of propagation, i.e. the z -axis. Other cases studied in this manuscript include forward SBS and inhomogeneous strain fields (e.g. due to temperature gradients or lattice mismatch) instead of the sketched geometry variations.

I. INTRODUCTION

Stimulated Brillouin Scattering (SBS) is a nonlinear and self-amplifying interaction between guided optical waves and hypersound waves in waveguides [1, 2]. The scattering of light from mechanical vibrations was first predicted by Brillouin in 1922 [3]; the stimulated version of this process was first experimentally demonstrated [4] shortly after the invention of the laser by Chiao et al. and has since been used successfully to characterize materials at hypersonic frequencies [5]. Following the general trend of miniaturization, SBS has been studied and applied in ever smaller structures such as nano-structured optical fibres [6] and even waveguides integrated on a chip [7]. In these systems SBS ceases to be a bulk effect and surface effects strongly come into play—most prominently radiation pressure appears as a second major interaction process in addition to the bulk photoelastic effect. Due to this additional coupling as well as the very tight mode confinement, high SBS-gains can be achieved in integrated waveguides [8–11], which makes them extremely interesting for signal processing applications [12] as well as narrow linewidth light sources [13]. Recently the idea of coherent phonon generation in phonon-lasers has gained considerable interest [14]. However, all these potential applications require or at least greatly benefit from the extremely narrow linewidth of the SBS process; line width broadening is highly detrimental in many cases [10, 11]. This motivates our investigation of the inhomogeneous line broadening due to structural variations of the waveguide and potential connections to the SBS-gain itself.

The finite phonon life time (or equivalently in backward SBS: the phonon propagation length) defines an intrinsic line width of the SBS-resonance. However, it has been known for some time that various imperfections of the SBS-system can distort the resonance and inhomogeneously broaden it. Some of these imperfections such as insufficient acoustic guidance in combination with moderate optical mode confinement [15] (one possible explanation for SBS broadening in optical fibres, but somewhat debated in this context) or simply the finite length of suspended nanowires [16] are inherent to some waveguide designs and cannot be avoided. In addition, local deviations from the intended ideal geometry can always lead to local variations in the Stokes shift. As a result, the total SBS-response of a non-ideal waveguide is the convolution of the intrinsic resonance and the Stokes frequency distribution along the waveguide. Incidentally, the geometry-dependence of the local Stokes shift has been used to measure the homogeneity of optical fibres [17] and to increase the SBS-threshold [18]. However, to date no connection has been made between the SBS-gain and the sensitivity of the Stokes shift, although this is suggested by the close connection between SBS and opto-mechanics [19], in which in turn the coupling strength is known to be closely related to the deformation-sensitivity of the optical subsystem [20].

The aim of this paper is to understand the impact of smooth and slowly varying perturbations of the waveguide structure (as sketched in Fig. 1). We include variations of the waveguide geometry and internal strain fields that change smoothly along the waveguide and on a length scale greater than the acoustic decay length. This is opposed to surface roughness, which is usually a major concern in fabrication, since it causes linear optical propagation loss via Rayleigh scattering—in backward SBS an analogous scattering of mechanical waves also contributes to the acoustic loss. In contrast, adiabatic structural variations do not scatter travelling waves and do not cause linear loss. However, they locally modify the dispersion relations and thereby influence the relative phase between the three waves participating in the SBS-process. Here, we show that one mechanism for this is through the optical dispersion relation and the sensitivity is closely connected to the SBS-gain, whereas the second mechanism is via the mechanical dispersion relation and completely independent from the SBS-gain. We show that these two mechanisms influence forward and backward SBS quite differently and that increasing the SBS-gain either by increasing the acousto-optic coupling or reducing the mechanical damping leads to a regime where the line width is dominated by structural

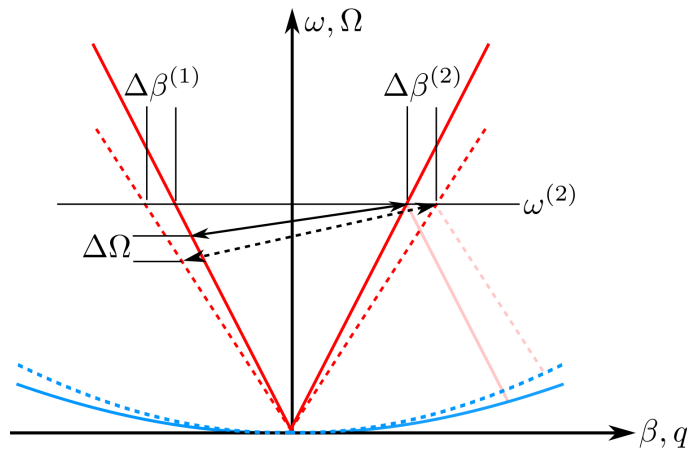


FIG. 2. Sketch of how a perturbation of the optical and acoustic dispersion relations (red and medium blue, respectively) affects the Stokes shift via the phase matching condition for constant pump frequency $\omega^{(2)}$. The double-arrow highlights the opto-acoustic transition that fulfils the conservation of both energy and momentum. The solid lines represent the dispersion relations of the ideal system and the dashed lines those of the perturbed system. The light pink lines are parallels of the respective left side optical branches and indicate which acoustic wave number is phase matched. Note that the magnitude of $\Delta\Omega$ is grossly exaggerated compared to $\omega^{(2)}$.

variations. The total SBS-response is then reduced to the square root of the intrinsic SBS-gain. We derive our results rigorously within the classical variant of a recent Hamiltonian formulation of SBS [21].

Throughout this manuscript we adhere to the notation and conventions introduced in our earlier paper on coupled-mode theory of SBS [22]. In Section II, we qualitatively describe the relation between SBS and the sensitivity of the dispersion relations and the resulting impact on the SBS-resonance. Although very useful for an intuitive understanding, this discussion lacks the quantitative precision of the formal derivation provided in Section III. The results of that section are then analytically studied in Section IV, focusing on the two important special cases of backward SBS and intra-mode forward SBS. Next, we study the relative importance of the two broadening mechanisms in forward and backward SBS in Section V using a family of suspended silicon nanowires as an example and find that they can compensate each other in appropriately engineered waveguides. Section VI summarises and concludes the paper.

II. QUALITATIVE DESCRIPTION

The acoustic properties of a waveguide are modified by static structural perturbations via mechanical nonlinearities, which are usually not relevant for the dynamics of optically generated sound waves. More precisely, there are separate contributions from internal strain fields and from variations of the cross section. Strain fields enter via the nonlinear relation between stiffness and stress:

$$T_{ij} = \sum_{kl} c_{ijkl} S_{kl} + \sum_{klmn} f_{ijklmn} S_{kl} S_{mn}, \quad (1)$$

where S and T are the strain and stress tensors, c is the conventional linear stiffness tensor and f is a second order nonlinear stiffness tensor (see Section III). At the same time, internal strain fields also modify the mass density distribution, because the trace of the strain tensor corresponds to a volume dilatation. Finally, changes in the cross section geometry cause a change in the boundary conditions (to be more specific: in the position of the boundary, not in the type of condition imposed there) of the acoustic Helmholtz equation. As an example, a slight reduction of the waveguide width might increase or decrease the acoustic frequency Ω depending on whether the acoustic mode is predominantly longitudinal or transversal and on whether the boundaries are approximately free or clamped.

At the same time, structural perturbations modify the optical properties of the waveguide. In contrast to the aforementioned acoustic frequency shift this modification is closely related to the SBS-process, which consists of two complementary nonlinear processes: the acoustic wave is excited by optical forces that are created by the beat of the optical pump and Stokes waves. The sound wave spatio-temporally varies the waveguide's optical properties and modulates the pump wave such that the Stokes side band is amplified. It is clear that the second process can only be efficient if the waveguide's dispersion relation is sensitive to small mechanical perturbations; if it was insensitive

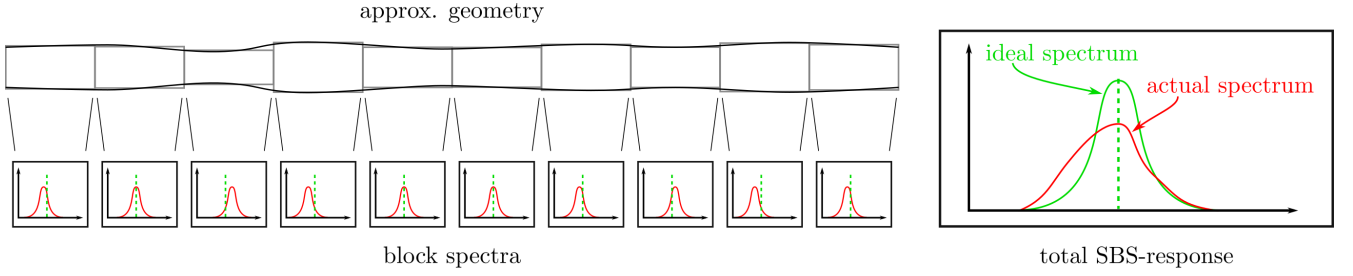


FIG. 3. Sketch of how a spatial distribution of the acoustic resonance frequency causes an inhomogeneously broadened SBS-response of the total waveguide. The waveguide is approximated by a sequence of homogeneous waveguide sections, each with its individual SBS-resonance centered around a frequency that might differ from the ideal frequency indicated by vertical dashed lines. The total response (right panel) is the superposition of all block responses and noticeably broader and shallower than the response of the ideal structure if the acoustic frequency variance is comparable to the resonance line width.

the acoustic wave would not modulate the pump wave. This cannot be compensated by a stronger excitation of the sound wave (neglecting irreversible forces), because both processes are described by the same mode overlap integral, hence are equally strong. However, the optical dispersion relation cannot distinguish between static and dynamic (i.e. acoustic) mechanical perturbations. Therefore, the optical properties of any waveguide that exhibits strong SBS are intrinsically sensitive to small structural perturbations introduced in the fabrication process. More precisely, waveguides whose SBS is mainly caused by photoelasticity are predominantly sensitive to internal strain fields, e.g. caused by inhomogeneous cooling of the sample, whereas waveguides whose SBS is mainly caused by radiation pressure are predominantly sensitive to slight variations of the waveguide cross section.

The variation of the optical dispersion relation occurs as a function of z rather than time, breaking the conservation of optical momentum. Therefore, this variation results in a change in the optical wave numbers $\beta^{(1)}$ and $\beta^{(2)}$ while leaving the optical frequencies unchanged. As a result, the pump frequency $\omega^{(2)}$ is exactly constant along the waveguide and the frequency $\omega^{(1)} = \omega^{(2)} - \Omega$ of the perfectly phase-matched Stokes wave varies only as a result of variations in the acoustic frequency Ω . These optical wave number variations translate to variations of the acoustic wave number through the momentum matching condition

$$q = \beta^{(2)} - \beta^{(1)}. \quad (2)$$

Therefore, the optical dispersion relation sensitivity indirectly affects the acoustic frequency. This effect has been practically applied in certain types of SBS-based fibre sensors [17, 23, 24]. The total local change in the acoustic frequency (see also Fig. 2) is given by the combination of the optical wave number variations and the direct acoustic shift $\Delta\Omega^{\text{dir}}$ described earlier:

$$\Delta\Omega^{\text{tot}} = \Delta\Omega^{\text{dir}} + \underbrace{\frac{\partial\Omega}{\partial q}(\Delta\beta^{(2)} - \Delta\beta^{(1)})}_{\Delta\Omega^{\text{indir}}}. \quad (3)$$

It should be noted at this point that the two contributions to the total frequency change can have opposite sign and therefore cancel (see Sec. V for an example).

In a waveguide that is subject to inhomogeneous variations of the geometry and strain fields the acoustic frequency variation becomes a function of the position z within the waveguide. It is instructive to imagine the waveguide to be composed of many short and approximately homogeneous sections (see Fig. 3). Each such section acts as an independent SBS-amplifier with a Stokes frequency that is offset from the ideal by $\Delta\Omega^{\text{tot}}(z)$. All other properties such as intrinsic line width and differential SBS-gain (i.e. the SBS gain per unit length of waveguide measured in units of $\text{W}^{-1}\text{m}^{-1}$) can be assumed to be unchanged. The total SBS-spectrum of the complete waveguide is then simply the superposition of the individual SBS-spectra. In the limit of very short homogeneous sections, within an undepleted pump approximation and assuming a Lorentzian intrinsic resonance shape, the Stokes amplification on resonance is then the integral:

$$\mathcal{A}_{\text{dB}}(\Omega) = \int_0^L dz \Gamma^{\text{ideal}}(\Omega - \Delta\Omega^{\text{tot}}(z))P^{(2)} = \Gamma^{\text{ideal}}(\Omega)P^{(2)} \int_0^L \frac{dz}{1 + [2\tau\Delta\Omega^{\text{tot}}(z)]^2}, \quad (4)$$

where τ represents the phonon life time and the waveguide is assumed to extend from $z = 0$ to $z = L$. Within the integral, Γ^{ideal} is the local (differential) SBS power gain measured in $\text{W}^{-1}\text{m}^{-1}$ (corresponding to the quantity g in

Boyd's book [1]) and $\mathcal{A}_{\text{dB}}^{\text{ideal}}(\Omega)$ is the total amplification accumulated over the total waveguide length L (denoted G by Boyd). If the distribution $\Delta\Omega^{\text{tot}}(z)$ has a width of the order τ^{-1} and especially if it is lopsided, the SBS-resonance is inhomogeneously broadened into a non-Lorentzian shape as indicated in Fig. 3.

So far, we have qualitatively explained the two main effects of structural variations on the SBS-resonance: perturbations to the acoustic and the optical dispersion relation and we have furthermore argued that the magnitude of the latter effect must be closely related to the SBS-gain. For practical purposes, it is probably sufficient to compute $\Delta\Omega^{\text{dir}}$ and $\Delta\beta^{(1,2)}$ numerically and insert them into Eqs. (3,4). However, the exact relationship between optical sensitivity and SBS-gain as well as further consequences can only be elucidated by a formal derivation. This is therefore the topic of the next section.

III. QUANTITATIVE DERIVATION

We assume SBS in a lossless optical waveguide that is oriented along the z -direction and provides confinement for the optical and all relevant acoustic modes, which are furthermore assumed to be only weakly damped. Mostly out of convenience we restrict ourselves to mechanically isotropic materials. Furthermore, we assume that the optical and acoustic envelopes as well as the deviations from the ideal waveguide geometry vary slowly along the z -axis compared to the acoustic decay length. We mostly follow the notation and conventions established in our earlier paper [22]: upper case letters refer to physical (real-valued) quantities, lower case letters to eigenmodes and envelope functions, and a tilde implies that the quantity is subjected to a phase transformation (rotating frame). We furthermore introduce the symbol $\eta = \varepsilon_r^{-1}$ for the inverse permittivity and the superscripts “bulk” and “edge” to refer to the interior of the waveguide's cross section and its boundary, respectively. We use Einstein's summation convention where it helps to simplify the notation.

A. Hamiltonian

We formulate this problem within a classical Hamiltonian framework. To this end, we transfer a recent comprehensive quantum-mechanical description of SBS [21] to the classical domain by replacing operators with functions and commutators with Poisson brackets. One of the main results of Ref. [21] is the full acousto-optic Hamiltonian, which reads in classical form:

$$H = \sum_{ijkl} \int d^3r \left[\frac{\Pi_i \Pi_i}{2\rho(\mathbf{r}; \mathbf{U})} + \frac{1}{2} S_{ij} c_{ijkl}(\mathbf{r}; \mathbf{U}) S_{kl} \right] + \sum_{ij} \int d^3r \left[\frac{B_i B_i}{2\mu_0} + \frac{D_i \eta_{ij}(\mathbf{r}; \mathbf{U}) D_j}{2\varepsilon_0} \right] = \int dz \mathcal{H}(z), \quad (5)$$

where $\mathcal{H}(z)$ is the Hamiltonian z -density, i.e. the Hamiltonian per unit length of waveguide. The mechanical displacement, strain and momentum density fields and the electric and magnetic induction fields are denoted with \mathbf{U} , S_{ij} , $\mathbf{\Pi}$, \mathbf{D} and \mathbf{B} , respectively. The material properties are described by the mass density ρ , the stiffness tensor c_{ijkl} , the inverse relative permittivity tensor $\eta = \varepsilon_r^{-1}$; the electromagnetic terms furthermore involve the permittivity ε_0 and permeability μ_0 of vacuum. All material constants are assumed to depend on the mechanical displacement field \mathbf{U} as well as its derivatives. The first integral describes the mechanical part of the system, whereas the second integral covers both the electromagnetic part and the acousto-optic interaction term, which is implicitly contained in the dependence of the inverse permittivity η on the mechanical deformation field and its derivatives. The two main contributions [21] to this dependence are

$$\eta_{ij} \approx \eta_{ij}^{\text{ideal}}(\mathbf{r} - \mathbf{U}(\mathbf{r})) + \sum_{kl} p_{ijkl}(\mathbf{r}) S_{kl}(\mathbf{r}); \quad (6)$$

a further term of linear order in \mathbf{U} – the moving polarization term described in Ref. [22] – is usually too weak to be observable and is neglected here. Within this framework we describe structural perturbations as a static contribution to the total mechanical displacement field \mathbf{U} :

$$\eta_{ij} \approx \eta_{ij}^{\text{ideal}}(\mathbf{r} - \mathbf{U}^{\text{stat}} - \mathbf{U}^{\text{dyn}}) + \sum_{kl} p_{ijkl} (S_{kl}^{\text{stat}} + S_{kl}^{\text{dyn}}), \quad (7)$$

where the superscripts “stat” and “dyn” denote the static and acoustic contributions, η^{ideal} is the permittivity distribution of the ideal (perfectly fabricated, sound-free) system and p_{ijkl} is the Pockels tensor that describes the photoelastic effect. Eq. (7) reflects the close connection between the acousto-optic interaction and the sensitivity of the optical dispersion relation regarding structural perturbations.

Similarly, the mechanical stiffness and the mass density depend on the mechanical displacement field:

$$\rho(\mathbf{r}) \approx \rho^{\text{ideal}}(\mathbf{r} - \mathbf{U}(\mathbf{r})) - \sum_i \rho^{\text{ideal}}(\mathbf{r}) S_{ii}(\mathbf{r}), \quad (8)$$

$$c_{ijkl}(\mathbf{r}) \approx c_{ijkl}^{\text{ideal}}(\mathbf{r} - \mathbf{U}(\mathbf{r})) + \sum_{mn} f_{ijklmn}(\mathbf{r}) S_{mn}(\mathbf{r}). \quad (9)$$

Here, the trace of the strain tensor expresses the volume dilatation. The strain-dependent stiffness tensor presented in (9) contains the leading order nonlinearity of mechanically isotropic bulk materials; microscopically, the sixth rank tensor f_{ijklmn} describes three-phonon scattering. This can also be derived within the classical framework of hyperelasticity [25]: in that approach, the stress is introduced as the strain-derivative of a free energy that is not quadratic in the strain variable. Assuming a purely reversible mechanical response, this free energy is identical to the Hamiltonian, whose strain-dependence can be expanded into a Taylor series. The leading (cubic) anharmonic strain-term is created by the sixth rank tensor f_{ijklmn} when inserting Eq. (9) into Eq. (5). In reality, this three-photon process might be forbidden by symmetry and a higher-order multi-phonon scattering would constitute the leader order of mechanical bulk nonlinearity. Furthermore, we have no reliable information about the order of magnitude of static strain fields across the large number of realisable integrated waveguides. Still, we have introduced this three-phonon term to illustrate how mechanical bulk nonlinearities would impact inhomogeneous broadening, although we neglect them in our analysis in Section IV.

Nonlinear mechanical wave processes usually can be neglected in typical SBS setups, so we only retain the static contributions to the mechanical nonlinearity:

$$\rho(\mathbf{r}) \approx \rho^{\text{ideal}}(\mathbf{r} - \mathbf{U}^{\text{stat}}) - \sum_i \rho^{\text{ideal}}(\mathbf{r}) S_{ii}^{\text{stat}}, \quad (10)$$

$$c_{ijkl}(\mathbf{r}) \approx c_{ijkl}^{\text{ideal}}(\mathbf{r} - \mathbf{U}^{\text{stat}}) + \sum_{mn} f_{ijklmn}(\mathbf{r}) S_{mn}^{\text{stat}}. \quad (11)$$

These terms describe the sensitivity of the acoustic dispersion relation to structural perturbations.

We now decompose the total Hamiltonian z -density into the unperturbed mechanical and electromagnetic parts (\mathcal{H}^{ac} , \mathcal{H}^{opt}), the interaction term \mathcal{V}^{int} and the structural perturbations \mathcal{V}^{opt} and \mathcal{V}^{ac} :

$$\mathcal{H} = \mathcal{H}^{\text{opt}} + \mathcal{H}^{\text{ac}} + \mathcal{V}^{\text{int}} + \mathcal{V}^{\text{opt}} + \mathcal{V}^{\text{ac}}, \quad (12)$$

where the first three terms are derived in Ref. [21]:

$$\mathcal{H}^{\text{ac}} = \int d^2r \frac{\Pi_i \Pi_i}{2\rho^{\text{ideal}}} + \frac{1}{2} S_{ij} c_{ijkl}^{\text{ideal}} S_{kl}, \quad (13)$$

$$\mathcal{H}^{\text{opt}} = \int d^2r \frac{B_i B_i}{2\mu_0} + \frac{D_i \eta_{ij}^{\text{ideal}}(\mathbf{r}) D_j}{2\varepsilon_0}, \quad (14)$$

$$\mathcal{V}^{\text{int}} = \int d^2r \frac{D_i D_j}{2\varepsilon_0} (p_{ijkl} S_{kl}^{\text{dyn}} - U_l^{\text{dyn}} \partial_l \eta_{ij}^{\text{ideal}}). \quad (15)$$

The integrals are carried out over the entire transverse plane. The fourth term is formed in direct analogy to \mathcal{V}^{int} :

$$\mathcal{V}^{\text{opt}} = \int d^2r \frac{D_i D_j}{2\varepsilon_0} (p_{ijkl} S_{kl}^{\text{stat}} - U_l^{\text{stat}} \partial_l \eta_{ij}^{\text{ideal}}), \quad (16)$$

and the last term is

$$\mathcal{V}^{\text{ac}} = \int d^2r \frac{S_{ij} S_{kl}}{2} (f_{ijklmn} S_{mn}^{\text{stat}} - U_m^{\text{stat}} \partial_m c_{ijkl}^{\text{ideal}}) - \frac{\Pi_i \Pi_i}{2(\rho^{\text{ideal}})^2} (S_{jj}^{\text{stat}} \rho^{\text{ideal}} - U_j^{\text{stat}} \partial_j \rho^{\text{ideal}}). \quad (17)$$

The difference between \mathcal{V}^{int} and \mathcal{V}^{opt} is that the former results in a nonlinear coupling term of the optical and acoustic equations of motion, whereas the latter causes a linear perturbation of the wave propagation within the optical fields. The fifth term \mathcal{V}^{ac} does not have a counterpart, because we neglected nonlinear wave effects within the propagating mechanical waves.

B. Modal expansion and approximation

Next, we expand the electromagnetic and mechanical fields into the eigenmode bases of the respective idealized waveguide problems [21, 22]

$$(\nabla_{\perp} + i\beta^{(i)}\hat{z}) \times (\nabla_{\perp} + i\beta^{(i)}\hat{z}) \times \tilde{\mathbf{e}}^{(i)} = \varepsilon\mu_0 [\omega^{(i)}]^2 \tilde{\mathbf{e}}^{(i)}; \quad (18)$$

$$(\nabla_{\perp} + iq\hat{z})_j c_{ijkl} (\nabla_{\perp} + iq\hat{z})_k \tilde{u}_l = -\rho\Omega^2 \delta_{il} \tilde{u}_l. \quad (19)$$

In both equations the wave numbers along the waveguide serve as parameters, where the optical wave number $\beta^{(2)}$ has to be chosen such that $\omega^{(2)}$ matches the frequency of the modelled pump laser and the acoustic wave number is subsequently found through Eq. (2). In very extended systems such as conventional optical fibres, an infinite number of acoustic basis functions can contribute to the total acoustic SBS response. In this case the treatment by Beugnot et al. [26] is a viable alternative to our description. However, we here restricted ourselves to nano-scale waveguides, in which the spectral separation between acoustic modes is greater than the SBS linewidth, i.e. in which only one or very few acoustic eigenmodes can be simultaneously excited by the two optical waves. Consequently, we express the optical and acoustic fields as modulations of single basis functions [22]

$$\mathbf{E}(\mathbf{r}, t) = \tilde{\mathbf{e}}^{(1)} \tilde{a}^{(1)}(z, t) \exp(i\beta^{(1)}z) + \tilde{\mathbf{e}}^{(2)} \tilde{a}^{(2)}(z, t) \exp(i\beta^{(2)}z) + \text{c.c.}, \quad (20)$$

$$\mathbf{U}^{\text{dyn}}(\mathbf{r}, t) = \tilde{\mathbf{u}}(\mathbf{r}, t) \tilde{b}(z, t) \exp(iqz) + \text{c.c.} \quad (21)$$

Here, $\tilde{a}^{(n)}$ and \tilde{b} are the classical counterparts of the quickly rotating envelope functions in Ref. [21] and are related to the more common slowly varying envelope functions $a^{(n)}$ and b via the relations

$$\tilde{a}^{(n)}(z, t) = a^{(n)}(z, t) \exp(-i\omega^{(n)}t), \quad (22)$$

$$\tilde{b}(z, t) = b(z, t) \exp(-i\Omega t). \quad (23)$$

They fulfil the Poisson bracket relations

$$\left\{ \tilde{a}^{(i)}(z, t), \tilde{a}^{(j)}(z', t') \right\} = \left\{ \tilde{a}^{(i)}(z, t), \tilde{b}(z', t') \right\} = \left\{ \tilde{a}^{(i)}(z, t), \tilde{b}^*(z', t') \right\} = 0, \quad (24)$$

$$\left\{ [\tilde{a}^{(i)}(z, t)]^*, \tilde{a}^{(j)}(z', t') \right\} = \frac{i\omega^{(i)}}{\mathcal{E}^{(i)}} \delta_{ij} \delta(z - z') \delta(t - t'), \quad (25)$$

$$\left\{ \tilde{b}^*(z, t), \tilde{b}(z', t') \right\} = \frac{i\Omega}{\mathcal{E}_b} \delta(z - z') \delta(t - t'). \quad (26)$$

The symbols \mathcal{E} denote the respective modal energies per unit length of waveguide [22]:

$$\mathcal{E}^{(i)} = 2\varepsilon_0 \sum_{kl} \int d^2r [\tilde{e}_k^{(i)}]^* \varepsilon_{kl}^{\text{ideal}} \tilde{e}_l^{(i)}, \quad (27)$$

$$\mathcal{E}_b = 2\Omega^2 \int d^2r \rho^{\text{ideal}} |\tilde{\mathbf{u}}|^2. \quad (28)$$

Within the expansions (20,21) the unperturbed contributions to the Hamiltonian z -density simply become

$$\mathcal{H}^{\text{opt}}(z) + \mathcal{H}^{\text{ac}}(z) = |\tilde{a}^{(1)}|^2 \mathcal{E}^{(1)} + |\tilde{a}^{(2)}|^2 \mathcal{E}^{(2)} + |\tilde{b}|^2 \mathcal{E}_b. \quad (29)$$

Using the fact that the acoustic eigenmodes (indexed by superscript n) for a fixed wave number q form a complete function set, we can expand the static deformations:

$$\mathbf{U}^{\text{stat}}(\mathbf{r}) = \sum_n \xi^{(n)}(z) \tilde{\mathbf{u}}^{(n)}(x, y) + \text{c.c.}; \quad (30)$$

$$S_{ij}^{\text{stat}}(\mathbf{r}) = \sum_n \xi^{(n)}(z) \tilde{s}_{ij}^{(n)}(x, y) + \text{c.c.}; \quad (31)$$

$$\text{with } \tilde{s}_{ij}^{(n)} = \frac{1}{2} \left[\partial_i \tilde{u}_j^{(n)} + \partial_j \tilde{u}_i^{(n)} \right]. \quad (32)$$

In this we have introduced separate expansions for the distribution of a static strain field and the deviation of the waveguide geometry, which contains both effects of the static strain field and variations of the geometry due to

fabricational (e.g. photolithography or etching) imperfections. In analogy to Refs. [21, 22], we now introduce separate modal overlap integrals to capture the effects of photoelasticity and of boundary displacement:

$$Q_{ij;p}^{\text{bulk}} = \varepsilon_0 \int_{\text{bulk}} d^2r \sum_{klmn} \varepsilon_r^2 [e_k^{(i)}]^* e_l^{(j)} p_{klmn} \partial_m [u_n^{(p)}]^*; \quad (33)$$

$$Q_{ij;p}^{\text{edge}} = \int_{\text{edge}} d\mathbf{r} \left[(\varepsilon_a - \varepsilon_b) \varepsilon_0 (\hat{n} \times \mathbf{e}^{(i)})^* (\hat{n} \times \mathbf{e}^{(j)}) - (\varepsilon_a^{-1} - \varepsilon_b^{-1}) \varepsilon_0^{-1} (\hat{n} \cdot \mathbf{d}^{(i)})^* (\hat{n} \cdot \mathbf{d}^{(j)}) \right] (\hat{n} \cdot \mathbf{u}^{(p)})^*. \quad (34)$$

Now, by substituting the modal expansions in (20,21) and (30,31) into the interaction terms in (15,16), and integrating over the transverse plane, we find the interactions can be reduced to the forms

$$\mathcal{V}^{\text{int}}(z) = a^{(1)} [a^{(2)}]^* b \underbrace{\left(Q_{12;n_b}^{\text{bulk}} + Q_{12;n_b}^{\text{edge}} \right)}_{Q_{\text{SBS}}} + \text{c.c.} \quad (35)$$

$$\mathcal{V}^{\text{opt}}(z) = \sum_n |a^{(1)}|^2 \left(\zeta^{(n)} Q_{11;n}^{\text{bulk}} + \xi^{(n)} Q_{11;n}^{\text{edge}} \right) + |a^{(2)}|^2 \left(\zeta^{(n)} Q_{22;n}^{\text{bulk}} + \xi^{(n)} Q_{22;n}^{\text{edge}} \right), \quad (36)$$

where n_b is the index of the phase-matched acoustic mode. The edge contribution $Q_{ij;n}^{\text{edge}}$ to the perturbation term \mathcal{V}^{opt} is of course identical to the expression by Johnson [27]. Finally, we analogously express the acoustic structural perturbation term

$$\mathcal{V}^{\text{ac}}(z) = |b|^2 \sum_n \left(\zeta^{(n)} R_n^{\text{bulk}} + \xi^{(n)} R_n^{\text{edge}} \right), \quad (37)$$

in terms of a bulk overlap integral

$$R_p^{\text{bulk}} = \frac{1}{2} \int_{\text{bulk}} d^2r \sum_{imn} \left\{ \sum_{jkl} [\partial_i u_j^{(n_b)}]^* [\partial_k u_l^{(n_b)}] f_{ijklmn} + \frac{\Omega^2 |u_i^{(n_b)}|^2}{2\rho^{\text{ideal}}} \right\} \left(\partial_m u_n^{(p)} + \partial_n e_m^{(p)} \right), \quad (38)$$

which directly corresponds to the photoelastic perturbation overlap $Q_{ij;n}^{\text{bulk}}$ and an edge integral R_p^{edge} that corresponds to the electromagnetic boundary displacement overlap $Q_{ij;n}^{\text{edge}}$. The explicit expression for R_p^{edge} is slightly involved and requires a short derivation; both can be found in Appendix A. Mathematically, this term contains the edge contributions from Eq. (17), i.e. the spatial derivatives of the stiffness and mass density functions. Physically, it describes the simple fact that the transverse acoustic pattern—which is a standing wave in the transversal plane—is detuned very much like a drumhead upon size variations of the transverse acoustic cavity.

Using the Poisson bracket relations, expanding the z -integral of the Hamiltonian density into the appropriate Taylor series [21] and truncating the expansion to first order, we find the equations of motion:

$$\partial_t \tilde{a}^{(i)} = \left\{ \tilde{a}^{(i)}, \mathcal{H}^{\text{opt}} \right\} + \left\{ \tilde{a}^{(i)}, \mathcal{V}^{\text{int}} + \mathcal{V}^{\text{opt}} \right\} \quad (39)$$

$$= -i\omega^{(i)} \tilde{a}^{(i)} - v^{(i)} \partial_z \tilde{a}^{(i)} + \left\{ \tilde{a}^{(i)}, \mathcal{V}^{\text{int}} + \mathcal{V}^{\text{opt}} \right\}; \quad (40)$$

$$\partial_t \tilde{b} = \left\{ \tilde{b}, \mathcal{H}^{\text{ac}} \right\} + \left\{ \tilde{b}, \mathcal{V}^{\text{int}} + \mathcal{V}^{\text{ac}} \right\} \quad (41)$$

$$= -i\Omega \tilde{b} - v_b \partial_z \tilde{b} + \left\{ \tilde{b}, \mathcal{V}^{\text{int}} + \mathcal{V}^{\text{ac}} \right\}. \quad (42)$$

C. Inhomogeneous broadening in steady state

We now have all tools to compute the spectrum of the steady state SBS response of an imperfect waveguide using the acoustic Green function [22]. To this end, we assume a small signal approximation and a local acoustic response approximation, for which we assume that the modal envelopes $a^{(1)}$, b as well as the perturbation envelopes $\zeta^{(n)}$, $\xi^{(n)}$ vary slowly compared to the acoustic decay length, which is of the order $\alpha^{-1} \approx 50 \mu\text{m}$ in backward SBS and is negligible in intra-mode forward SBS. Following Ref. [22], we introduce the inverse acoustic decay length α as well as an additional parameter κ that describes a wave number offset between the ideally phase-matched Stokes mode

and the probe wave that is injected in a seeded small-signal SBS-experiment. The Poisson brackets involving the perturbation terms (36,37) are:

$$\{a^{(i)}, \mathcal{V}^{\text{opt}}\} = i v^{(i)} \Delta \beta^{(i)} a^{(i)}, \quad (43)$$

$$\{b, \mathcal{V}^{\text{ac}}\} = i v_b \Delta q^{\text{dir}}, \quad (44)$$

expressed in terms of the structural detuning parameters

$$\Delta \beta^{(i)}(z) = \frac{\omega^{(i)}}{\mathcal{P}^{(i)}} \sum_n \left(\zeta^{(n)} Q_{ii;n}^{\text{bulk}} + \xi^{(n)} Q_{ii;n}^{\text{edge}} \right); \quad (45)$$

$$\Delta q^{\text{dir}}(z) = \frac{\Omega}{\mathcal{P}_b} \sum_n \left(\zeta^{(n)} R_n^{\text{bulk}} + \xi^{(n)} R_n^{\text{edge}} \right). \quad (46)$$

The steady state equations then follow:

$$\partial_z a^{(1)} - i(\Delta \beta^{(1)} + \kappa) a^{(1)} = - \frac{i \omega^{(1)} Q_{\text{SBS}}}{\mathcal{P}^{(1)}} a^{(2)} b^* \quad (47)$$

$$\partial_z a^{(2)} - i \Delta \beta^{(2)} a^{(2)} = - \frac{i \omega^{(2)} Q_{\text{SBS}}^*}{\mathcal{P}^{(2)}} a^{(1)} b \quad (48)$$

$$\partial_z b + (\alpha - i \Delta q^{\text{dir}}) b = - \frac{i \Omega Q_{\text{SBS}}}{\mathcal{P}_b} [a^{(1)}]^* a^{(2)}, \quad (49)$$

with the SBS coupling parameter $Q_{\text{SBS}} = Q_{12;n_b}^{\text{bulk}} + Q_{12;n_b}^{\text{edge}}$ from Eq. (35) and the powers $\mathcal{P}^{(i)} = v^{(i)} \mathcal{E}^{(i)}$ and $\mathcal{P}_b = b_b \mathcal{E}_b$ of the eigenmodes as introduced in Ref. [22]. We then solve the acoustic equation using its Green function:

$$b(z) = - \frac{i \Omega Q_{\text{SBS}}}{\mathcal{P}_b} \int_0^\infty dz' \left\{ [a^{(1)}(z - z')]^* a^{(2)}(z - z') \exp(-[\alpha - i \Delta q^{\text{dir}}(z - z')] z') \right\}.$$

We assumed that the optical intensities as well as the structural envelopes vary slowly on the length scale α^{-1} , so we can assume that the $\Delta q^{\text{dir}}(z)$, $\Delta \beta^{(1)}(z)$, $\Delta \beta^{(2)}(z)$ and the absolute values $|a^{(1)}|$ and $|a^{(2)}|$ are constant within the convolution (50); κ is simply a constant. We may therefore approximate the product of optical envelopes at the position $z - z'$ as that product at position z modulo a phase factor that expresses the relative beat $\Delta \beta^{(2)} - \Delta \beta^{(1)} - \kappa$:

$$[a^{(1)}(z - z')]^* a^{(2)}(z - z') \approx [a^{(1)}(z)]^* a^{(2)}(z) \exp(i[\Delta \beta^{(2)}(z) - \Delta \beta^{(1)}(z) - \kappa] z'), \quad (50)$$

$$\Rightarrow b(z) \approx - \frac{i \Omega Q_{\text{SBS}}}{\mathcal{P}_b} [a^{(1)}(z)]^* a^{(2)}(z) L(z), \quad (51)$$

with

$$L(z) = \frac{1}{\alpha - i[\Delta q^{\text{tot}}(z) - \kappa]} \quad (52)$$

$$\Delta q^{\text{tot}} = \Delta q^{\text{dir}} - \Delta \beta^{(1)} + \Delta \beta^{(2)}. \quad (53)$$

We can now insert this expression for the acoustic field into the optical equations. Along the lines of Ref. [22], we then transform them into a pair of equations for the optical powers $P^{(i)}(z) = \mathcal{P}^{(i)} |a^{(i)}(z)|^2$:

$$\partial_z P^{(1)} = \Gamma(z) P^{(1)} P^{(2)}, \quad (54)$$

$$\partial_z P^{(2)} = - \Gamma(z) P^{(1)} P^{(2)}. \quad (55)$$

The local SBS-gain function is given by

$$\Gamma(z) = \underbrace{\frac{2 \omega \Omega |Q_{\text{SBS}}|^2}{\mathcal{P}^{(1)} \mathcal{P}^{(2)} \mathcal{P}_b \alpha}}_{\Gamma^{\text{ideal}}} \cdot \frac{\alpha^2}{\alpha^2 + [\Delta q^{\text{tot}}(z) - \kappa]^2}. \quad (56)$$

Within a small signal approximation, i.e. $\partial_z P^{(2)} \approx 0$, this leads to a separable equation for the Stokes power $P^{(1)}$:

$$\frac{\partial_z P^{(1)}}{P^{(1)}} = \Gamma(z) P^{(2)}; \quad (57)$$

$$\Rightarrow P^{(1)}(z) = P^{(1)}(0) \exp \left[P^{(2)} \int_0^z dz' \Gamma(z') \right], \quad (58)$$

and an expression for the total Stokes amplification $\mathcal{A}_{\text{dB}} = 10 \log_{10}(P_{\text{out}}^{(1)}/P_{\text{in}}^{(1)})$ dB of the waveguide of length L :

$$\boxed{\mathcal{A}_{\text{dB}} = \frac{10}{\log 10} P^{(2)} \Gamma^{\text{ideal}} \int_0^L dz' \frac{\alpha^2}{\alpha^2 + [\Delta q^{\text{tot}}(z') - \kappa]^2}} \quad (59)$$

in units of dB.

In the simple case of z -independent aberration coefficients $\zeta^{(n)}$ and $\xi^{(n)}$ the integral in Eq. (59) becomes equal to one if the detuning κ is chosen to be $\kappa = \Delta q^{\text{tot}}$. This means that to an excellent approximation the acoustic frequency and thereby the SBS-resonance is simply shifted by the frequency

$$\Delta \Omega^{\text{tot}} = v_b \Delta q^{\text{tot}} = \underbrace{v_b \Delta q^{\text{dir}}}_{\Delta \Omega^{\text{dir}}} + \underbrace{v_b (\Delta \beta^{(2)} - \Delta \beta^{(1)})}_{\Delta \Omega^{\text{indir}}}, \quad (60)$$

in agreement with Eq. (3). In the case of inhomogeneous coefficients, the integral in Eq. (59) expresses the linear superposition of individual SBS-resonances and therefore the inhomogeneous resonance broadening in agreement with Eq. (4).

IV. SPECIAL CASES

We will now study the two practically most relevant special cases: intra-mode forward SBS and backward SBS. Qualitatively, inter-mode scattering behaves similarly to backward SBS.

A. Forward intra-mode SBS

First, we study the case of forward intra-mode SBS, i.e. we assume

$$\mathbf{e}^{(1)}(\vec{r}, t) \approx \mathbf{e}^{(2)}(\vec{r}, t); \quad (61)$$

$$q \approx 0; \quad v_b \approx 0. \quad (62)$$

In this case, the SBS coupling coefficient is

$$Q_{\text{SBS}} = Q_{11;n_b}^{\text{bulk}} + Q_{11;n_b}^{\text{edge}}. \quad (63)$$

Furthermore, the optical wave number perturbations are identical:

$$\Delta \beta^{(2)} = \Delta \beta^{(1)} = \frac{\omega^{(1)}}{\mathcal{P}^{(1)}} \sum_n \left(\zeta^{(n)} Q_{11;n}^{\text{bulk}} + \xi_{11;n}^{(n)} \right). \quad (64)$$

As a result, $\Delta \Omega^{\text{indir}} = 0$, i.e. the indirect resonance broadening via the optical dispersion relation is absent in intra-mode forward SBS. Strictly speaking, this result is exact only if the optical group velocity is identical at $\omega^{(1)}$ and $\omega^{(2)}$; in practice this is irrelevant except for extremely dispersive optical modes, e.g. in the slow light regime near band edges. The remaining source of structural resonance broadening is the direct mechanical contribution

$$\Delta \Omega^{\text{dir}} = v_b \frac{\Omega}{\mathcal{P}_b} \sum_n \left(\zeta^{(n)} R_n^{\text{bulk}} + \xi^{(n)} R_n^{\text{edge}} \right) \quad (65)$$

$$= \frac{\Omega}{\mathcal{E}_b} \sum_n \left(\zeta^{(n)} R_n^{\text{bulk}} + \xi^{(n)} R_n^{\text{edge}} \right). \quad (66)$$

If we assume that internal strain fields are too weak to cause noticeable resonance broadening, we may assume

$$\Delta\Omega^{\text{dir}} = \frac{\Omega}{\mathcal{E}_b} \sum_n \xi^{(n)} R_n^{\text{edge}}, \quad (67)$$

i.e. that the resonance detuning can be regarded as the simple geometric effect of changing the size of a transversal acoustic cavity. The mechanical perturbation overlaps R and the acousto-optic overlaps Q are in principle completely independent, so there is no fundamental reason why an increase in the SBS-gain would increase the inhomogeneous broadening in the case of intra-mode forward SBS.

B. General backward SBS

This is fundamentally different in the case of backward SBS and (to a lesser extent) in the case of general inter-mode SBS. The optical modes that participate in conventional backward SBS are the counter-propagating partners of each other and therefore related via complex conjugation:

$$\mathbf{e}^{(1)}(\mathbf{r}, t) = [\mathbf{e}^{(2)}(\mathbf{r}, t)]^*; \quad \mathcal{P}^{(1)} = -\mathcal{P}^{(2)}. \quad (68)$$

Therefore, the SBS coupling coefficient and the optical wave number perturbations are:

$$Q_{\text{SBS}} = Q_{12;n_b}^{\text{bulk}} + Q_{12;n_b}^{\text{edge}}, \quad (69)$$

$$\Delta\beta^{(2)} = -\Delta\beta^{(1)} = \frac{\omega^{(1)}}{\mathcal{P}^{(1)}} \sum_n \left(\zeta^{(n)} Q_{11;n}^{\text{bulk}} + \xi^{(n)} Q_{11;n}^{\text{edge}} \right), \quad (70)$$

while the expression for the direct acoustic detuning is identical to the case of forward SBS. The subscript indices of the individual overlap integrals $Q_{ij;n}^{\text{bulk}}$ and $Q_{ij;n}^{\text{edge}}$ are the mode labels of the involved two optical and the acoustic mode [see Eqs. (33–34)]. It is in fact the acousto-optic forward-SBS coupling of the respective acoustic and optical modes, i.e. basically the square root of the forwards SBS gain for that combination of modes. This time, the optical wave number perturbations add up and the total Stokes shift becomes:

$$\Delta\Omega^{\text{tot}} = 2 \sum_n \left[\zeta^{(n)} \left(\frac{\Omega}{\mathcal{E}_b} R_n^{\text{bulk}} + \frac{v_b \omega^{(1)}}{v^{(1)} \mathcal{E}^{(1)}} Q_{11;n}^{\text{bulk}} \right) + \xi^{(n)} \left(\frac{\Omega}{\mathcal{E}_b} R_n^{\text{edge}} + \frac{v_b \omega^{(1)}}{v^{(1)} \mathcal{E}^{(1)}} Q_{11;n}^{\text{edge}} \right) \right]. \quad (71)$$

The direct mechanical contribution is qualitatively identical to the previous case. Furthermore, we can assume that the predominantly longitudinal acoustic mode contributing to backward SBS is rather insensitive to slight geometry variations. This suggests to focus on the indirect (optical) contribution to the broadening and ignore the direct (acoustic) contribution. As a result, the general result Eq. (59) then has the explicit form (i.e. $\kappa = 0$):

$$\mathcal{A}_{\text{dB}} = \frac{20 P^{(2)} \omega^{(1)} \Omega \alpha}{\mathcal{P}_b \log 10} \int_0^L dz \frac{\left| Q_{12;n_b}^{\text{bulk}} + Q_{12;n_b}^{\text{edge}} \right|^2}{\left(\alpha \mathcal{P}^{(1)} \right)^2 + \left(2 \omega^{(1)} \sum_n \zeta^{(n)}(z) Q_{11;n}^{\text{bulk}} + \xi^{(n)}(z) Q_{11;n}^{\text{edge}} \right)^2}. \quad (72)$$

The mode coefficients $Q_{11;n}^{\text{bulk}}$ and $Q_{11;n}^{\text{edge}}$ in the denominator are mode overlaps that define the forward SBS gain and are identical to the coefficients $Q_{12;n}^{\text{bulk}}$ and $Q_{12;n}^{\text{edge}}$ in the numerator except for a complex conjugation of one of the optical modes courtesy of Eq. (68).

C. Backward SBS dominated by radiation pressure

The general BSBS result Eq. (72) is too convoluted to interpret directly. We therefore restrict ourselves to a very specific limiting case that nonetheless provides some insight into the general impact of geometrical variations in BSBS in nanoscale waveguides. We assume that the acousto-optic interaction is dominated by the edge term $Q_{11;n}^{\text{edge}}$, i.e. by radiation pressure. We furthermore assume that the contributions $\xi^{(n_b)}$ of the phase matched acoustic mode to the geometry perturbations provide a good estimate for the total optical sensitivity $\Delta\beta^{(1)}$. We finally assume that the geometry variations are completely random within a certain interval. Within this approximation $\xi^{(n_b)}(z)$ is uniformly

distributed in an interval $[-\xi_0, \xi_0]$; other distributions of $\xi^{(n_b)}(z)$ clearly lead to different broadened resonance shapes, but also exhibit the general trends described below. These assumptions reduce Eq. (72) to the much simpler form

$$\mathcal{A}_{\text{dB}} \approx \frac{5P^{(2)}\Omega\alpha}{\mathcal{P}_b\omega^{(1)}\log 10} \left| \frac{Q_{12;n_b}^{\text{edge}}}{Q_{11;n_b}^{\text{edge}}} \right|^2 \frac{1}{2\xi_0} \int_{-\xi_0}^{\xi_0} \frac{d\xi}{\Theta^2 + \xi^2} \quad (73)$$

$$\text{with } \Theta = \frac{\alpha\mathcal{P}^{(1)}}{2\omega^{(1)}Q_{11;n_b}^{\text{edge}}}. \quad (74)$$

For the case of strong broadening ($\Theta \ll \xi_0$) the integral approaches the limit

$$\frac{1}{2\xi} \int_{-\xi_0}^{\xi_0} \frac{d\xi}{\Theta^2 + \xi^2} \rightarrow \frac{\pi}{2\xi_0\Theta} = \frac{\pi\omega^{(1)}Q_{11;n_b}^{\text{edge}}}{\alpha\mathcal{P}^{(1)}\xi_0}, \quad (75)$$

and therefore the total amplification approaches the limit

$$\mathcal{A}_{\text{dB}} \rightarrow \underbrace{\frac{5\pi\Omega}{\mathcal{P}_b\mathcal{P}^{(1)}\log 10}}_{\text{constants}} \underbrace{\left| \frac{Q_{12;n_b}^{\text{edge}}}{Q_{11;n_b}^{\text{edge}}} \right|^2}_{\text{gain ratio}} \underbrace{\frac{P^{(2)}Q_{11;n_b}^{\text{edge}}}{\xi_0}}_{\text{scaling}}. \quad (76)$$

This result consists of a combination of eigenmode constants such as frequencies and mode powers, the ratio of the intrinsic forward and backward SBS gains and a term defining how the broadened SBS amplification scales with various design parameters, especially the fabrication tolerance ξ_0 . The gain ratio is always slightly below one, as we show in Appendix B, and we can simply assume it to be a constant. The last term finally scales with the inverse of the acoustic damping, the fabrication tolerance and $Q_{11;n_b}^{\text{edge}}$, which can be identified as being proportional to the square root of the FSBS power gain using Eq. (56) and Eq. (63). Alternatively, we can also formulate the result as scaling with the square root of the BSBS power gain by using

$$\left| \frac{Q_{12;n_b}^{\text{edge}}}{Q_{11;n_b}^{\text{edge}}} \right|^2 \frac{P^{(2)}Q_{11;n_b}^{\text{edge}}}{\xi_0} = \left| \frac{Q_{12;n_b}^{\text{edge}}}{Q_{11;n_b}^{\text{edge}}} \right| \frac{P^{(2)}|Q_{12;n_b}^{\text{edge}}|}{\xi_0}. \quad (77)$$

Both interpretations are basically equivalent, because FSBS and BSBS gain are closely related (Appendix B).

If we assume a waveguide with a significant SBS contribution due to radiation pressure and we assume the tolerance ξ_0 to be given, the reduction of Θ either by reducing the acoustic damping parameter α or by increasing the FSBS acousto-optic coupling $Q_{11;n_b}^{\text{edge}}$ will lead into a regime where the BSBS amplification is defined by $Q_{11;n_b}^{\text{edge}}$. In practice, the acoustic loss can be reduced e.g. by reducing the contact area of a nearly suspended waveguide to its substrate [11]; certain slot waveguide designs [28] on the other hand allow control of the radiation pressure coupling by varying the gap size.

V. NUMERICAL EXAMPLE

As the last part of our study, we performed numerical experiments on the sensitivity of the SBS frequency shift to variations of a waveguide's geometry. We selected a family of silicon nanowires with a height of 220 nm and a width varying between 300 nm and 450 nm in steps of 25 nm. For each such waveguide, we characterized forward and backward SBS between the fundamental optical mode and the two lowest symmetry-permitted acoustic modes [29] using the finite-element solver COMSOL with an element size of 5 nm inside the waveguide. For each step of 25 nm, we estimated the width sensitivity by increasing the width by 1 nm and repeating the calculation. The resulting relative frequency shifts are plotted as solid lines in the lower left panels of Fig. 4 and Fig. 6. Finally, we added computed SBS power gains of the respective acoustic modes as annotations to the SBS frequency graphs; they are intended to give a rough idea of the respective acousto-optic coupling.

In the case of FSBS (Fig. 4), the difference is entirely due to the direct (acoustic) perturbation effect, because the acoustic wave number is basically zero. Both acoustic modes are standing waves in the acoustic resonator, formed perpendicular to the axis of light propagation, where the first mode has contributions from both in-plane components of the mechanical displacement field and the second mode only contributions from the out-of-plane component. As a result, the second mode is a pure standing S-wave and consequently its eigenfrequency is entirely determined by the

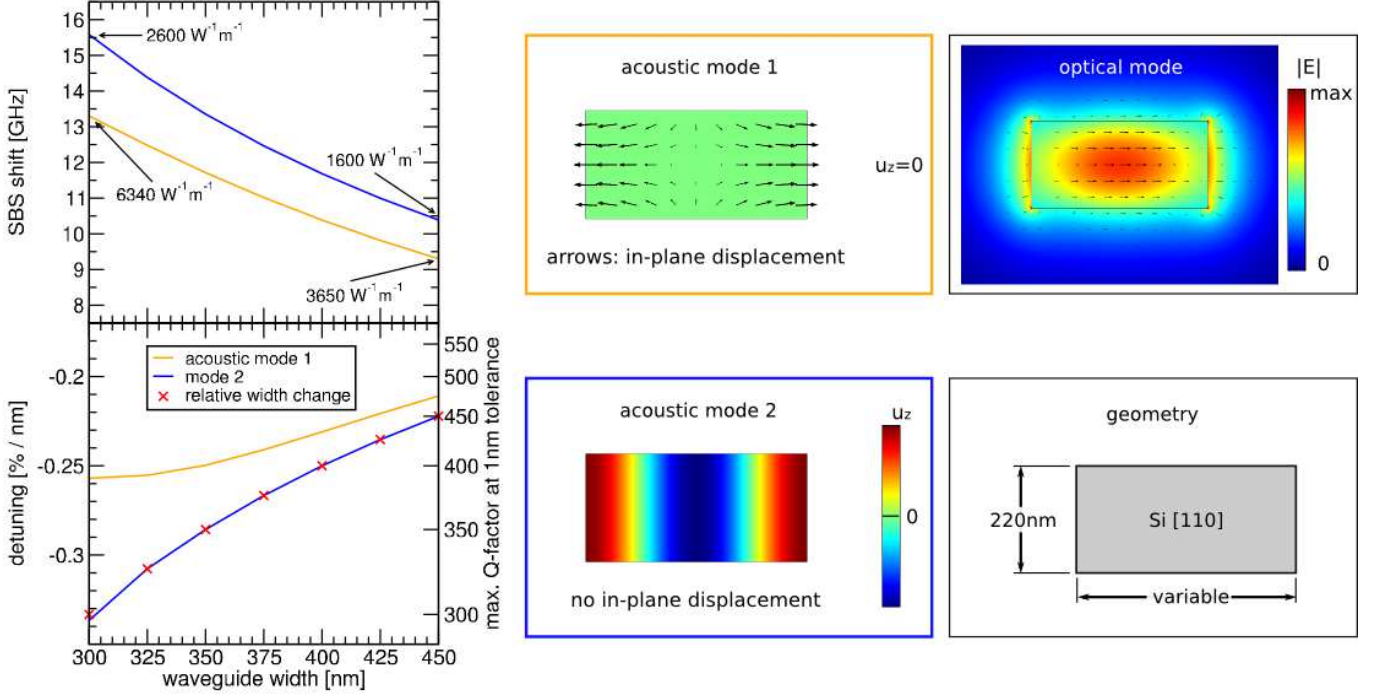


FIG. 4. Numerical study of the sensitivity of *forward* SBS (FSBS) to width variations of a silicon nanowire oriented in the [110] crystal direction. We study the interaction between the fundamental optical mode and two symmetry-permitted acoustic modes with lowest frequency. The acoustic mode patterns show the in-plane displacement components as arrows and the axial displacement coordinate via a color map. The first acoustic mode (orange frame and graph lines) does not have any axial contributions, whereas the second acoustic mode (blue frame and lines) has no in-plane contributions to the displacement field. The relative detunings are displayed in percent for a change of the waveguide width by 1 nm. Due to the extremely small acoustic wave number in FSBS only the direct acoustic perturbation process contributes to the resonance shift, whose relative magnitude follows the relative width change exactly for mode 2 and qualitatively for mode 1. This demonstrates the direct acoustic response to width changes is basically given by the detuning of the transverse mechanical cavity. The annotations in the top left panel specify the computed SBS power gains of the two acoustic modes for the extreme waveguide widths assuming a mechanical quality factor of 300.

waveguide width and the transverse speed of sound. This leads to the exact correspondence of the variation of Ω and the relative change of the waveguide width (red crosses in Fig. 4). In contrast, the first mode is a hybrid of an S-wave and a P-wave, because both in-plane components contribute. As a result, the relationship between waveguide width and Ω is not as straightforward. This mode for a waveguide width of 450 nm was studied experimentally in Ref. [11] and its sensitivity has been determined to be 20 MHz/nm at a measured Brillouin frequency of 9.2 GHz equivalent to a sensitivity of 0.22 %/nm in excellent agreement with Fig. 4. Still, Fig. 4 demonstrates that the geometry sensitivity of FSBS is only a response to size variations of a transverse acoustic resonator.

In addition, we have also computed broadened FSBS spectra of the first mode (computed frequency shift: 9.3 GHz at a width of 450 nm). Fig. 5 shows the impact of a width variation of ± 1 nm. This is a little less than two lattice constants of the silicon crystal, i.e. it corresponds roughly to two monolayers of atoms. Fig. 5 also illustrates the effect of different distributions of width variations along the waveguide. The leftmost panel shows the unperturbed spectrum assuming a mechanical quality factor of 300, which is a realistic value for certain FSBS experiments [11] where mechanical loss is dominated by acoustic leakage. The center panel shows the broadened spectrum assuming that the waveguide length linearly changes along the total waveguide length (typically several millimetres to centimetres); as a result the quality factor significantly drops to 183. The rightmost panel finally shows the broadened spectrum assuming that the waveguide width fluctuates sinusoidally along the waveguide with a period that is large compared to the acoustic decay length and the optical wave length (the exact periodicity does not matter). In this case, not only is the quality factor further reduced to 155, but the resonance is also deformed into a highly non-Lorentzian shape with two distinct peaks. This example shows that high effective quality factors in integrated SBS require very consistent fabrication down to the atom level.

For BSBS, the situation is slightly more complicated, because the indirect (optical) perturbation contributes to the total sensitivity. Therefore, we additionally determined the impact of the direct contribution by solving the acoustic

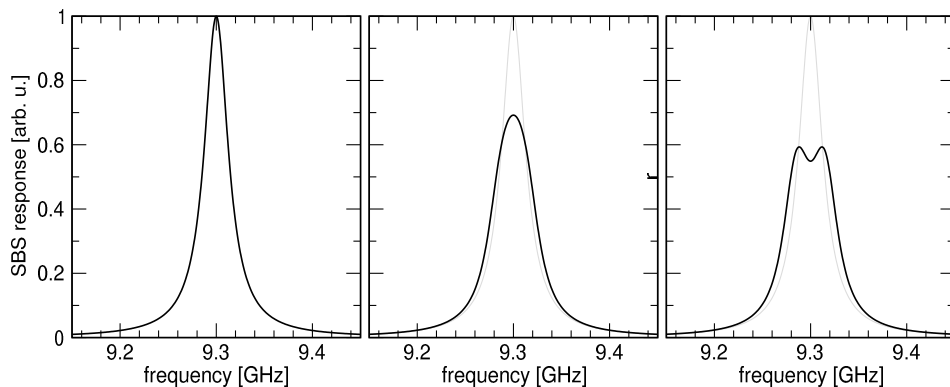


FIG. 5. Effect of geometry-induced broadening on an SBS resonance. The system is forward SBS in a suspended silicon nanowire of dimensions 220×450 nm at a mechanical quality factor of 300, i.e. the system studied in Fig. 4 and in Ref. [11]. The three panels show the unperturbed resonance (left panel), the line for the case that the width linearly varies from 449 to 451 nm over the waveguide length (center panel) and for the case that the waveguide width is sinusoidally undulated between the values 449 and 451 nm. In both cases, the perturbation reduces the quality factor by about a factor of two.

problem for the perturbed geometry and the wave number derived from the unperturbed problem (circles in Fig. 6); the indirect (optical) contribution (squares in Fig. 6) then follows as the difference. Both studied acoustic modes are hybrid and have an axial wave length that is comparable to the waveguide's dimensions. Therefore, the acoustic frequency is roughly determined by the bulk speed of sound and the wave number. The displacement field of the first acoustic mode has appreciable x -components, which leads to a noticeable direct (acoustic) sensitivity. In contrast, the second mode is mostly insensitive to the direct perturbation effect. Both acoustic modes are very susceptible to the indirect (optical) perturbation effect. For example, the second acoustic mode responds to a width variation of 1 nm with a resonance shift of up to 0.4%. Correspondingly, a waveguide with a width of 300 nm would have to be manufactured to better than 0.25 nm (less than a monolayer of atoms) along its entire length in order to maintain an overall quality factor of 1000. Evidence for this problem has been observed experimentally [30].

One interesting detail of Fig. 6 is the fact that the direct and indirect contributions to the inhomogeneous broadening can be of comparable magnitude. Furthermore, they will tend to have opposite signs, because an increase in waveguide width tunes the transverse acoustic resonator to lower frequencies via the direct (acoustic) perturbation mechanism, while an increase in the width also leads to higher optical mode indices, corresponding to greater wave numbers and eventually higher acoustic frequencies via the indirect (optical) perturbation mechanism. This suggests the very promising idea to design a waveguide structure with a deliberately *strong* direct sensitivity in order to cancel the inevitable indirect sensitivity. The result would be a waveguide design with greatly relaxed fabrication tolerances with respect to the waveguide width. The general applicability of this concept to minimise the sensitivity with respect to one design parameter (in this case the width) is proven by the behavior of mode 1 in Fig. 6. There, the direct and indirect contributions for width variations nearly cancel for small waveguide widths. However, the presented mode is only of academic interest because of its very low SBS power gain. Finally, it should be noted that only one specific type of perturbations (e.g. width variations, wall angle variations or height variations) can be compensated with this technique while potentially increasing the sensitivity of the other perturbation types.

VI. SUMMARY

In conclusion, we have analysed the sensitivity of the optical and acoustic dispersion relations on structural variations of a waveguide and related this to the sensitivity of the Stokes shift Ω . We have shown that variations of the optical dispersion relation are a major source of inhomogeneous broadening in backward SBS and that they are intimately related to the forward SBS coupling, because slowly and smoothly varying perturbations mainly modify the phase of an optical mode, and induce negligible back-scattering. This leads to a counter-intuitive result in SBS dominated by radiation pressure (see Section IV C): Since the inhomogeneous broadening is proportional to the forward SBS coupling (i.e. square root of FSBS-gain), the maximum of a strongly broadened SBS spectrum is proportional to the ratio of the backward gain and the square root of the forward gain. As a result the maximum of the strongly broadened response of a backward SBS system scales only with the square root of the naively expected SBS-gain.

This means that high-gain backward SBS waveguides are intrinsically sensitive to fabrication imperfections and require fabrication tolerances matched not only to the intrinsic acoustic line width but also to the opto-acoustic

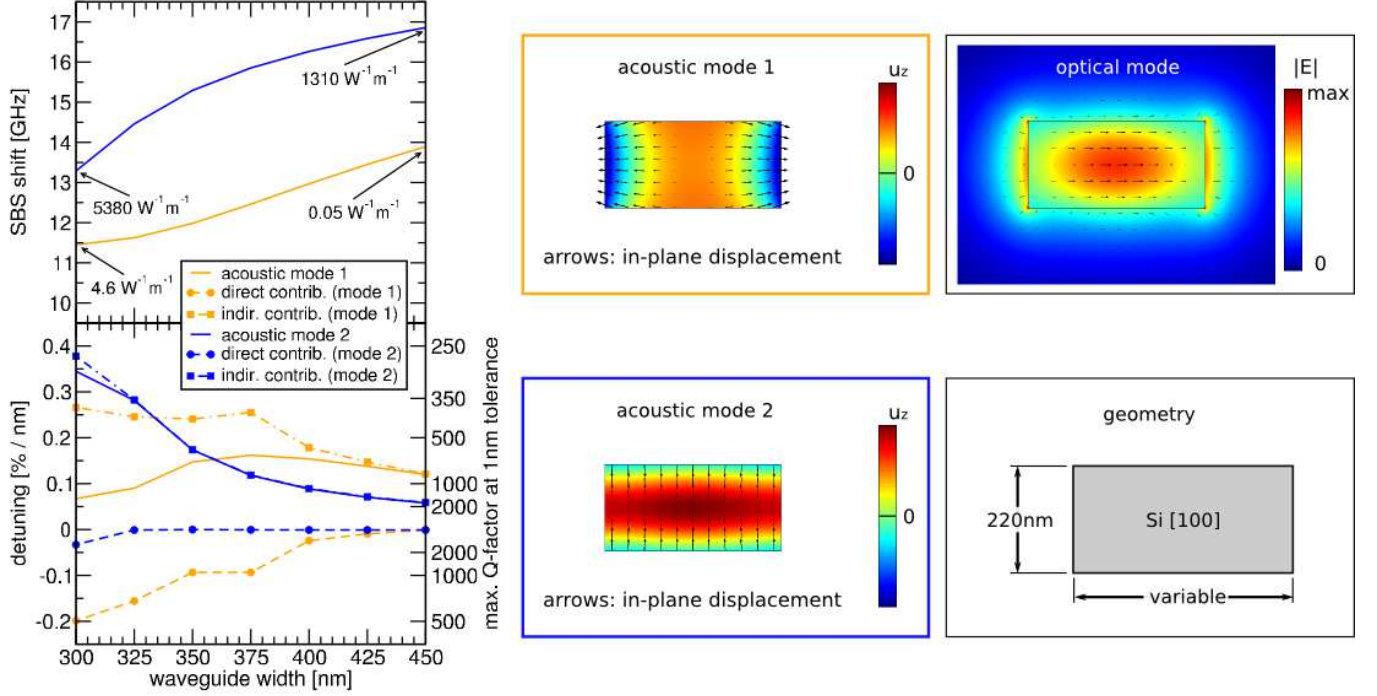


FIG. 6. Numerical study of the sensitivity of *backward* SBS (BSBS) to width variations of a silicon nanowire oriented in the [100] crystal direction. In contrast to FSBS (Fig. 4), both studied acoustic modes involve axial and in-plane components. Furthermore, BSBS features both the direct (acoustic) process (with negative sign as for FSBS) and in addition the indirect (optical) process with the opposite sign. The former can be neglected for wider waveguides; however, it is possible that both contributions cancel each other. As in Fig. 4 we annotated the power gain, this time assuming a quality factor of 1000. The extremely low power gain of mode 1 is caused by nearly exact u cancellation of the photoelastic and moving-boundary related coupling in this structure.

coupling strength. Therefore, it may be advisable in practice to sacrifice some intrinsic SBS-gain to avoid the tolerance-dominated regime, especially since this might reduce the linear or nonlinear optical loss at the same time and thereby increase the overall figure of merit. We have furthermore shown that the indirect resonance sensitivity is absent in forward SBS and that therefore no fundamental link between the resonance sensitivity and the SBS-gain exists in this case. Nonetheless, the direct (acoustic) resonance sensitivity can be appreciable and has been observed in at least one nanophotonic realisation of forward SBS [11]. Our numerical example for FSBS is in excellent agreement with this experiment. Finally, we have argued that the direct (acoustic) and indirect (optical) contributions to the resonance sensitivity tend to have opposite sign. This allows one to design comparatively insensitive high-gain waveguides with a strong direct sensitivity carefully engineered to compensate the intrinsic indirect sensitivity.

ACKNOWLEDGEMENTS

C.W., M.J.S., B.J.E. and C.G.P. acknowledge financial support from the Australian Research Council (ARC) via the Discovery Grant DP130100832, its Laureate Fellowship (B.J.E., FL120100029) program, and the ARC Center of Excellence CUDOS (CE110001018). R.V.L. acknowledges the Agency for Innovation by Science and Technology in Flanders (IWT) for a PhD grant.

Appendix A: Mechanical edge perturbations

In this appendix, we derive the edge contribution to the mechanical perturbation term. This is analogous to the perturbation theory developed by Johnson et al. for the perturbation of the electromagnetic dispersion relation [27], which is based on the continuity of the transversal electric field and of the normal electric induction field across a material boundary. In the context of continuum mechanics, the quantities that are continuous across a material

boundary are the normal projection of the stress tensor

$$T_{ij}^\perp = n_i \sum_k n_k T_{kj}, \quad (\text{A1})$$

and the in-plane projection of the strain tensor

$$S_{ij}^\parallel = S_{ij} - n_i \sum_k n_k S_{kj}, \quad (\text{A2})$$

where \hat{n} is the surface normal. In analogy to the electromagnetic case, the perturbation to the Hamiltonian is the normal projection of the surface displacement multiplied by the mechanical energy density expressed in terms of the conserved quantities, where we restrict ourselves to isotropic materials such as glasses or homogenised polycrystalline cubic materials (the expressions for anisotropic materials are more complex, but of the same general form). We introduce an auxiliary strain quantity

$$S_{ij}^{\text{eff}} = S_{ij}^\parallel + n_i \sum_{klm} n_k [c^{-1}]_{kjl m} T_{lm}^\perp, \quad (\text{A3})$$

where $[c^{-1}]$ is the mechanical compliance tensor. This allows us to write the acoustic perturbation overlap caused by boundary displacements in a concise form:

$$\mathcal{V}^{\text{ac,edge}} = \int_{\text{edge}} d\mathbf{r} \sum_{ijkl} [S_{ij}^{\text{eff}} c_{ijkl} S_{kl}^{\text{eff}}] (\hat{n} \cdot \mathbf{U}). \quad (\text{A4})$$

Within the modal expansion employed in Section III, the edge-effect of the p -th acoustic basis function of the phase matched acoustic mode n_b becomes:

$$R_p^{\text{edge}} = \int_{\text{edge}} d\mathbf{r} \sum_{ijkl} \left[(s_{ij}^{\text{eff}})^* c_{ijkl} s_{kl}^{\text{eff}} \right] (\hat{n} \cdot \mathbf{u}^{(p)})^*, \quad (\text{A5})$$

with the modal (note the lower case) generalisation of Eq. (A3)

$$s_{ij}^{\text{eff}} = \frac{1}{2} \left[\partial_i u_j^{(n_b)} + \partial_j u_i^{(n_b)} - n_i \sum_k n_k \left(\partial_k u_j^{(n_b)} + \partial_j u_k^{(n_b)} \right) \right. \\ \left. + n_i \sum_{klpq\alpha\beta} n_k [c^{-1}]_{kjl p} n_l n_q c_{pb\alpha\beta} \left(\partial_\alpha u_\beta^{(n_b)} + \partial_\beta u_\alpha^{(n_b)} \right) \right]. \quad (\text{A6})$$

Appendix B: Ratio of FSBS and BSBS radiation pressure terms

In this appendix we investigate the ratio between the acousto-optic coupling terms of forward and backward SBS. We find that they are always of the same order and that the radiation pressure coupling is always greater for forward SBS.

Inserting $\mathbf{e}^{(1)} = [\mathbf{e}^{(2)}]^* = \mathbf{e}$ into the explicit definitions Eqs. (33,34) the forward and backward coupling terms are:

$$Q_p^{\text{FSBS}} = Q_p^{\text{bulk,FSBS}} + Q_p^{\text{edge,FSBS}} = Q_{11;p}^{\text{bulk}} + Q_{11;p}^{\text{edge}} \quad (\text{B1})$$

$$= \varepsilon_0 \int_{\text{bulk}} d^2 r \sum_{klmn} \varepsilon_r^2 e_k^* e_l p_{klmn} \partial_m [u_n^{(p)}]^* \quad (\text{B2})$$

$$+ \int_{\text{edge}} d\mathbf{r} \left[(\varepsilon_a - \varepsilon_b) \varepsilon_0 (\hat{n} \times \mathbf{e}^* (\hat{n} \times \mathbf{e}) - (\varepsilon_a^{-1} - \varepsilon_b^{-1}) \varepsilon_0^{-1} (\hat{n} \cdot \mathbf{d})^* (\hat{n} \cdot \mathbf{d})) \right] (\hat{n} \cdot \mathbf{u}^{(p)})^*,$$

$$Q_p^{\text{BSBS}} = Q_p^{\text{bulk,BSBS}} + Q_p^{\text{edge,BSBS}} = Q_{12;p}^{\text{bulk}} + Q_{12;p}^{\text{edge}} \quad (\text{B3})$$

$$= \varepsilon_0 \int_{\text{bulk}} d^2 r \sum_{klmn} \varepsilon_r^2 e_k^* e_l p_{klmn} \partial_m [u_n^{(p)}]^* \quad (\text{B4})$$

$$+ \int_{\text{edge}} d\mathbf{r} \left[(\varepsilon_a - \varepsilon_b) \varepsilon_0 (\hat{n} \times \mathbf{e}^* (\hat{n} \times \mathbf{e}^*) - (\varepsilon_a^{-1} - \varepsilon_b^{-1}) \varepsilon_0^{-1} (\hat{n} \cdot \mathbf{d})^* (\hat{n} \cdot \mathbf{d}^*)) \right] (\hat{n} \cdot \mathbf{u}^{(p)})^*.$$

The only difference is the complex conjugation of the second optical mode. Due to the symmetry of Eqs. (18,19) the phases of the optical as well as the acoustic modes can be adjusted such that the in-plane field components are purely real-valued and the axial components are purely imaginary. Thus, the main effect of the complex conjugation is a sign reversal in the z -component of the second optical mode. In the photoelastic coupling term $Q_{ij;n}^{\text{bulk}}$ the axial components of one mode and the transversal components of another mode can be nontrivially combined depending on the orientation of the principal axes of p_{ijkl} relative to the waveguide geometry. However, the edge term $Q_{ij;n}^{\text{edge}}$ can be easily analysed. First we notice that the axial component of $\mathbf{u}^{(p)}$ is irrelevant. Next, we decompose the transversal electromagnetic fields into components normal and parallel to the waveguide surface:

$$e_{\perp} = \hat{n} \cdot \mathbf{e}; \quad (\text{B5})$$

$$e_{\parallel} = |\mathbf{e} - \hat{n}(\hat{n} \cdot \mathbf{e}) - \hat{z}(\hat{z} \cdot \mathbf{e})|. \quad (\text{B6})$$

Within this notation we find:

$$Q_p^{\text{edge,FSBS}} = \int_{\text{edge}} d\mathbf{r} \left[(\varepsilon_a - \varepsilon_b) \varepsilon_0 (|e_{\parallel}|^2 + |e_z|^2) + (\varepsilon_b^{-1} - \varepsilon_a^{-1}) \varepsilon_0^{-1} |d_{\perp}|^2 \right] (\hat{n} \cdot \mathbf{u}^{(p)})^*, \quad (\text{B7})$$

$$Q_p^{\text{edge,BSBS}} = \int_{\text{edge}} d\mathbf{r} \left[(\varepsilon_a - \varepsilon_b) \varepsilon_0 (|e_{\parallel}|^2 - |e_z|^2) + (\varepsilon_b^{-1} - \varepsilon_a^{-1}) \varepsilon_0^{-1} |d_{\perp}|^2 \right] (\hat{n} \cdot \mathbf{u}^{(p)})^*. \quad (\text{B8})$$

The factors $(\varepsilon_a - \varepsilon_b)$ and $(\varepsilon_b^{-1} - \varepsilon_a^{-1})$ always have the same sign (note the reversal of subscripts). Therefore, the radiation pressure contribution to the intra-mode forward SBS coupling is always greater than the corresponding contribution to the backward SBS coupling. This result does not apply to the photoelastic coupling.

-
- [1] R. W. Boyd, *Nonlinear optics* (Academic, 3rd ed., 2003).
 - [2] G. P. Agrawal, *Nonlinear fiber optics* (Academic, 5th ed., 2012).
 - [3] L. Brillouin. "Diffusion de la lumière par un corps transparent homogène," *Annals of Physics* **17**, 88–122 (1922).
 - [4] R. Y. Chiao, C. H. Townes, and B. P. Stoicheff, "Stimulated Brillouin scattering and coherent generation of intense hypersonic waves," *Phys. Rev. Lett.* **12**, 592 (1964).
 - [5] N. Uchida and N. Niizeki. "Acoustooptic Deflection Materials and Techniques," *Proc. IEEE* **61**, 1073–1092 (1973).
 - [6] P. Dainese, P. St. J. Russell, N. Joly, J. C. Knight, G. S. Wiederhecker, H. L. Fragnito, V. Laude, and A. Khelif, "Stimulated Brillouin scattering from multi-GHz-guided acoustic phonons in nanostructured photonic crystal fibres," *Nature Phys.* **2**, 388–392 (2006).
 - [7] B. J. Eggleton, C. G. Poulton, and R. Pant, "Inducing and harnessing stimulated Brillouin scattering in photonic integrated circuits," *Adv. Opt. Photonics* **5**, 536–587 (2013).
 - [8] R. Pant, C. G. Poulton, D.-Y. Choi, H. Mcfarlane, S. Hile, E. Li, L. Thévenaz, B. Luther-Davies, S. J. Madden, and B. J. Eggleton, "On-chip stimulated Brillouin scattering," *Opt. Express* **19**, 8285–8290 (2011).
 - [9] P. T. Rakich, C. Reinke, R. Camacho, P. Davids, and Z. Wang, "Giant enhancement of stimulated Brillouin scattering in the subwavelength Limit," *Phys. Rev. X* **2**, 011008 (2012).
 - [10] H. Shin, W. Qiu, R. Jarecki, J. A. Cox, R. H. O. Ill, A. Starbuck, Z. Wang, and P. T. Rakich, "Tailorable stimulated Brillouin scattering in nanoscale silicon waveguides," *Nature Commun.* **4**, 1944 (2013).
 - [11] R. Van Laer, B. Kuyken, D. Van Thourhout, and R. Baets, "Interaction between light and highly confined hypersound in a silicon photonic nanowire," *Nature Photon.* **9**, 199–203 (2015).
 - [12] S. Chin, L. Thévenaz, J. Sancho, S. Sales, J. Capmany, P. Berger, J. Bourderionnet, and D. Dolfi, "Broadband true time delay for microwave signal processing, using slow light based on stimulated Brillouin scattering in optical fibers," *Opt. Express* **18**, 22599–22613 (2010).
 - [13] K. S. Abedin, P. S. Westbrook, J. W. Nicholson, J. Porque, T. Kremp, and X. Liu, "Single-frequency Brillouin distributed feedback fiber laser," *Opt. Lett.* **37**, 605 (2012).
 - [14] I. S. Grudin, H. Lee, O. Painter, and K. J. Vahala, "Phonon Laser Action in a Tunable Two-Level System," *Phys. Rev. Lett.* **104**, 083901 (2010).
 - [15] V. I. Kovalev, and R. G. Harrison, "Waveguide-induced inhomogeneous spectral broadening of stimulated Brillouin scattering in optical fiber," *Opt. Lett.* **27**, 2022–2024 (2002).
 - [16] C. Wolff, M. J. Steel, B. J. Eggleton, and C. G. Poulton, "Acoustic build-up in on-chip stimulated Brillouin scattering," *Sci. Rep.* **5**, 13656 (2015).
 - [17] J.-C. Beugnot, M. Tur, S. Føleng Mafang, and L. Thévenaz, "Distributed Brillouin sensing with sub-meter spatial resolution: modeling and processing," *Opt. Express* **19**, 7381–7397 (2011).
 - [18] B. Stiller, A. Kudlinski, Min Won Lee, G. Bouwmans, M. Delqué, J.-C. Beugnot, H. Maillotte, and T. Sylvestre, "SBS Mitigation in a Microstructured Optical Fiber by Periodically Varying the Core Diameter," *IEEE Photon. Technol. Lett.* **24**, 667–669 (2012).

- [19] R. Van Laer, B. Kuyken, R. Baets, D. Van Thourhout “Unifying Brillouin scattering and cavity optomechanics, ” *arXiv:1503.03044 [physics.optics]*, (2015).
- [20] M. Aspelmeyer, T. J. Kippenberg, and F. Marquardt, “Cavity optomechanics, ” *Rev. Mod. Phys.* **86**, 1391–1452 (2014).
- [21] J. Sipe, and M. J. Steel “A Hamiltonian treatment of stimulated Brillouin scattering in nanoscale integrated waveguides,” *arXiv:1509.01017 [physics.optics]*, (2015).
- [22] C. Wolff, M. J. Steel, B. J. Eggleton, and C. G. Poulton, “Stimulated Brillouin Scattering in integrated photonic waveguides: forces, scattering mechanisms and coupled mode analysis,” *Phys. Rev. A* **92**, 013836 (2015).
- [23] T. Horiguchi, K. Shimizu, T. Kurashima, M. Tateda, Y. Koyamada, “Development of a distributed sensing technique using Brillouin scattering,” *J. Lightwave Technol.*, **13**, 1296–1302 (1995).
- [24] M. Nikles, L. Thevenaz, P. A. Robert, “Simple distributed fiber sensor based on Brillouin gain spectrum analysis,” *Opt. Lett.* **21**, 758-760 (1996).
- [25] D. Bigoni *Nonlinear Solid Mechanics* (Cambridge, 2012).
- [26] J.-C. Beugnot, V. Laude, “Electrostriction and guidance of acoustic phonons in optical fibers,” *Phys. Rev. B* **86**, 224304 (2012).
- [27] S. G. Johnson, M. Ibanescu, M. A. Skorobogotiy, O. Weisberg, J. D. Joannopoulos, Y. Fink, “Perturbation theory for Maxwell’s equations with shifting material boundaries,” *Phys. Rev. E* **65**, 066611 (2002).
- [28] R. Van Laer, B. Kuyken, D. Van Thourhout, and R. Baets, “Analysis of enhanced stimulated Brillouin scattering in silicon slot waveguides,” *Opt. Lett.* **39**, 1242-1245 (2014).
- [29] C. Wolff, M. J. Steel, C. G. Poulton, “Formal selection rules for Brillouin scattering in integrated waveguides and structured fibers,” *Opt. Express* **22**, 32489-32501 (2014).
- [30] R. Van Laer, A. Bazin, B. Kuyken, R. Baets, D. Van Thourhout, “Net on-chip Brillouin gain based on suspended silicon nanowires,” *New. J. Phys.* **17**, 115005 (2015).